Stochastic Environmental Research and Risk Assessment
https://doi.org/10.1007/s00477-019-01660-8

ORIGINAL PAPER

Multiple-point statistical simulation of the ore boundaries for a lateritic bauxite deposit

Y. Dagasan[1] · O. Erten[2] · P. Renard[1] · J. Straubhaar[1] · E. Topal[2]

Abstract
Resource estimation of mineral deposits requires spatial modelling of orebody boundaries based on a set of exploration borehole data. Given lateritic bauxite deposits, the spacing between the boreholes is often determined based on the grade continuity. As a result, the selected drill spacing might not capture the underlying (true) lateral variability apparent in the orebody boundaries. The purpose of this study is to investigate and address the limitations imposed by such problems in lateritic metal deposits through multiple-point statistics (MPS) framework. Rather than relying on a semivariogram model, we obtain the required structural information from the footwall topographies exposed after previous mining operations. The investigation utilising the MPS was carried out using the Direct Sampling (DS) MPS algorithm. Two historical mine areas along with their mined-out surfaces and ground penetrating radar surveys were incorporated as a bivariate training image to perform the MPS simulations. In addition, geostatistical simulations using the Turning Bands method were also performed to make the comparison against the MPS results. The performances were assessed using several statistical indicators including higher-order spatial cumulants. The results have shown that the DS can satisfactorily simulate the orebody boundaries by using prior information from the previously mined-out areas.

Keywords Multiple-point statistics · Direct sampling · Bauxite mining · Stratified · Laterite · Geostatistics · Resource estimation

1 Introduction

The ultimate goal of resource estimation practice is to accurately predict the grades and tonnages of a mineral deposit that will be exploited during a specified time frame (Rossi and Deutsch 2013; Bardossy et al. 2003). Such a goal requires one to define the geological boundaries within which block models are constructed to estimate the orebody attributes (i.e., thickness, grade). A traditional practice to achieve this is to explicitly draw the boundaries using the borehole data (Osterholt and Dimitrakopoulos 2018). This method can be rather subjective and results in an over-smoothed interpretation of the geology. Alternative means to model the geological domains include geostatistical estimation techniques, such as kriging (de Freitas Silva and Dimitrakopoulos 2016). However, there exists several drawbacks of incorporating geostatistical interpolation techniques in orebody modelling. As for the kriging method, such drawbacks comprise the smoothing effect and failure to reproduce complex non-linear geological structures (Rezaee et al. 2015). In addition, kriging estimates cannot be used for the uncertainty assessment, as they do not reflect the true variability (variogram). Due to the issues pointed out, use of kriging to delineate the orebody boundaries may pose risks in resource estimations and mine planning (Bastante et al. 2008).

Conditional simulation techniques address the above-mentioned issues by generating equi-probable realisations of the orebody variability (Dimitrakopoulos 1998). Each

Electronic supplementary material The online version of this article (https://doi.org/10.1007/s00477-019-01660-8) contains supplementary material, which is available to authorized users.

✉ Y. Dagasan
yasin.dagasan@postgrad.curtin.edu.au

[1] Centre for Hydrogeology and Geothermics, University of Neuchâtel, Rue Emile-Argand 11, 2000 Neuchâtel, Switzerland

[2] Department of Mining and Metallurgical Engineering, Western Australian School of Mines, Curtin University, Kalgoorlie, WA 6430, Australia

Published online: 21 February 2019

orebody realisation reproduces the original statistical properties and the variogram inferred from the borehole observations. In other words, these realisations do not undergo any smoothing effect as in kriging. Moreover, when taken together, they can serve as a measure of uncertainty associated with the orebody boundaries. However, the geostatistical simulation techniques rely on a variogram or a covariance model, which fails to capture non-linear complex physical realities (Journel 2005; Mariethoz and Caers 2014; De Iaco and Maggio 2011). Besides, since the structural information to perform the simulations is often derived from the borehole data, the spatial continuity cannot always be accurately inferred in the case of a limited data set, which is the case mostly seen in reservoir modelling studies.

Multiple-point statistics (MPS) offers a variety of tools to perform stochastic reconstruction of spatial data. It provides a framework to go beyond the two-point statistics through the Training Image (TI) concept. A TI can be considered as an analogue of a variogram model in traditional geostatistics. It serves as a conceptual geological model containing spatial patterns which are thought to exist in the simulation domain (Mariethoz and Caers 2014). MPS simulations utilise the patterns from the TI to perform the simulations through a number of MPS simulation algorithms (Guardiano and Srivastava 1992; Strebelle 2002; Zhang et al. 2006; Arpat and Caers 2007; Gloaguen and Dimitrakopoulos 2009; Dimitrakopoulos et al. 2010; Honarkhah and Caers 2010; Mariethoz et al. 2010; Straubhaar et al. 2011; Tahmasebi et al. 2012).

The use of TIs in orebody modelling can provide some benefits. For instance, a chosen TI contains high-order structural information that cannot be adequately expressed in terms of second-order statistics. Therefore, borrowing the structural information from a TI allows reproducing realistic and complex orebody structures. Secondly, utilisation of a TI as structural information alleviates the issues associated with the limited conditioning data sets. Rather than relying on the borehole data to derive the structural information, such spatial information is borrowed from the TI containing rich spatial patterns. Lastly, since a TI is a non-mathematical definition of the structural information, it is rather user-friendly (Mariethoz and Caers 2014).

Although MPS has frequently been used in the oil and gas industry, its applications in mineral deposits are still not as widespread (Pasti et al. 2012). One of the major causes is the challenge faced when deriving an appropriate TI which is representative of the geology of interest (Mery et al. 2017). Nevertheless, some approaches have previously been adopted to construct a TI for mineral deposits. An example of these is the utilisation of the exploration or blasthole drills to interpret the geology (Jones et al. 2013). Furthermore, deterministic orebody models which are created by utilising drill holes are also used as training images (van der Grijp and Minnitt 2015; Goodfellow et al. 2012; Pérez et al. 2014; Robles-Stefoni and Dimitrakopoulos 2016). Another approach is to derive the geological model from the previously mined-out areas (Rezaee et al. 2013; Osterholt and Dimitrakopoulos 2018). Lastly, if the characteristics of the geological structures are known, conceptual geological models generated by TI generator software can also be used (Pasti et al. 2012; Bastante et al. 2008).

This study investigates the applicability of MPS to model the footwall topography, which delineates the ore/waste interface in a lateritic bauxite deposit. The main difference between our MPS application and the ones presented above is the source of the TI used. As contrary to the previous mining MPS applications, we do not utilise an interpreted, modelled or generated TI. Instead, we obtain the TI directly from the mined-out surface exposed after the extraction of a certain portion of an analogue mining area in the same mine site. Since the bauxite extraction is carried out by tracing the footwall topography at the time of mining, the resulting mined-out floor can be deemed representative of the spatial variations seen in a future mining area. In other words, we exploit and test one of the fundamental ideas of MPS; which is to use data from analogue sites that can be considered as ex-situ prior. Another difference in our application is the type of the variables used. Most of the MPS applications in mining consider categorical variables. We, instead, work with two continuous variables representing the elevation of the footwall topography and its estimation by ground penetrating radar in a multivariate framework. Therefore, this study presents a new approach to simulate the orebody boundaries using MPS. The overall workflow is presented on a case study using a dataset from a lateritic bauxite deposit. The step-by-step description of the methodology comprises the stages from data preparation to simulation. The resulting MPS simulations are compared with more classical geostatistical simulations in terms of spatial statistical indicators.

2 Laterite-type bauxite mining and motivation to use MPS

Resource estimation of a lateritic bauxite deposit is usually performed using sparsely-spaced boreholes drilled on a regular grid within the modelling domain (Abzalov and Bower 2014; Erten 2012). The selected drill spacing between these drill holes is based predominantly on the variation and continuity in grades (Hartman and Mutmansky 2002). Hence, the defined drill spacing is sufficient to model the alumina Al_2O_3% grade within the bauxite unit.

However, as the geological interface between the bauxite and ironstone units varies more than the grade, the chosen drill spacing fails to adequately infer the lateral variability in the footwall contact topography (Dagasan 2018; Erten 2012; Dagasan et al. 2018a; Erten et al. 2013, 2015). Therefore, contact models created using interpolation techniques, such as the ones offered by geostatistics, become less detailed and smoother than the reality. An example of orebody boundaries created using such boreholes can be seen in Fig. 1.

Due to the reasons mentioned above, the orebody boundaries cannot be accurately defined. As a result, the mining equipment operator becomes unable to rely on a predefined ore boundary when extracting the deposit. Instead, the operator utilises the hardness and colour differences between successive geological units to track the ore boundaries. After extracting the bauxite ore, a mined-out surface is exposed for each mining area within the mine site. An example of such an exposed mined-out topography can be seen in Fig. 2.

Although the shape of the resulting topography is influenced by the mining equipment selectivity and the operator's skills, it is thought to reflect the actual lateral variability of the geological contact between the bauxite and the underlying ferricrete unit. Motivated by this fact, a mine floor exposed from a previously mined-out area can be used as a TI to model the footwall topography of another mining area with a similar geology.

3 Methodology

The overall methodology is composed of several steps, which can be seen in Fig. 3. The details of the steps are given in the below sections.

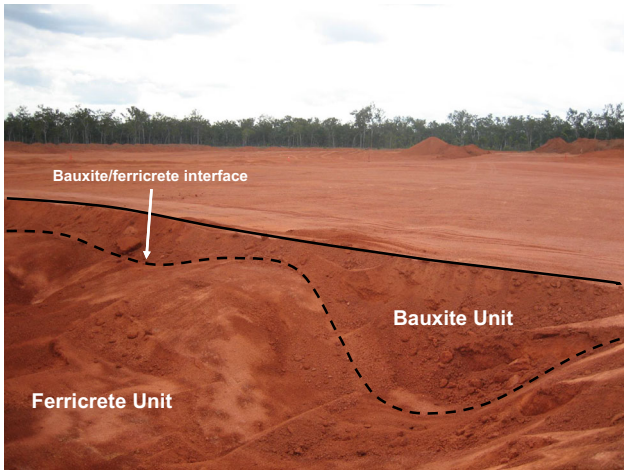

Fig. 2 An example mined-out topography exposed following the extraction of the bauxite ore. After Erten (2012)

3.1 Data description and pre-processing

Two lateritic bauxite mine areas located within the same mine site, namely Oak and Kumbur, were used to investigate the implementation of MPS for the lateritic metal mines in this research. Prior to the extraction of the bauxite ore, several types of exploration data sets were collected to model the deposits. These data sets include (1) exploration boreholes, (2) production control boreholes (PCB) and (3) dense ground penetrating radar (GPR) survey data to help locate the ore boundaries.

GPR surveys provide a non-invasive means of subsurface imaging by utilising the differences between the bauxite and the underlying ferricrete layer (Davis and Annan 1989). The GPR device used in this study had antennas with 80 MHz central frequency. The data was collected in the north–south and east–west parallel continuous profiles, as can also be seen in Fig. 4. The spacing

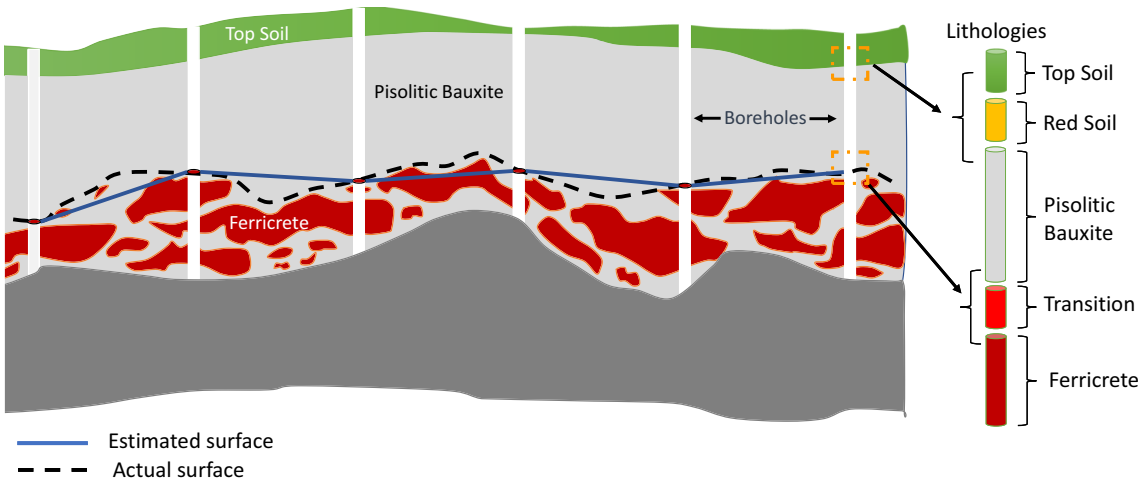

Fig. 1 Orebody boundaries created using sparse borehole data set. After Erten (2012)

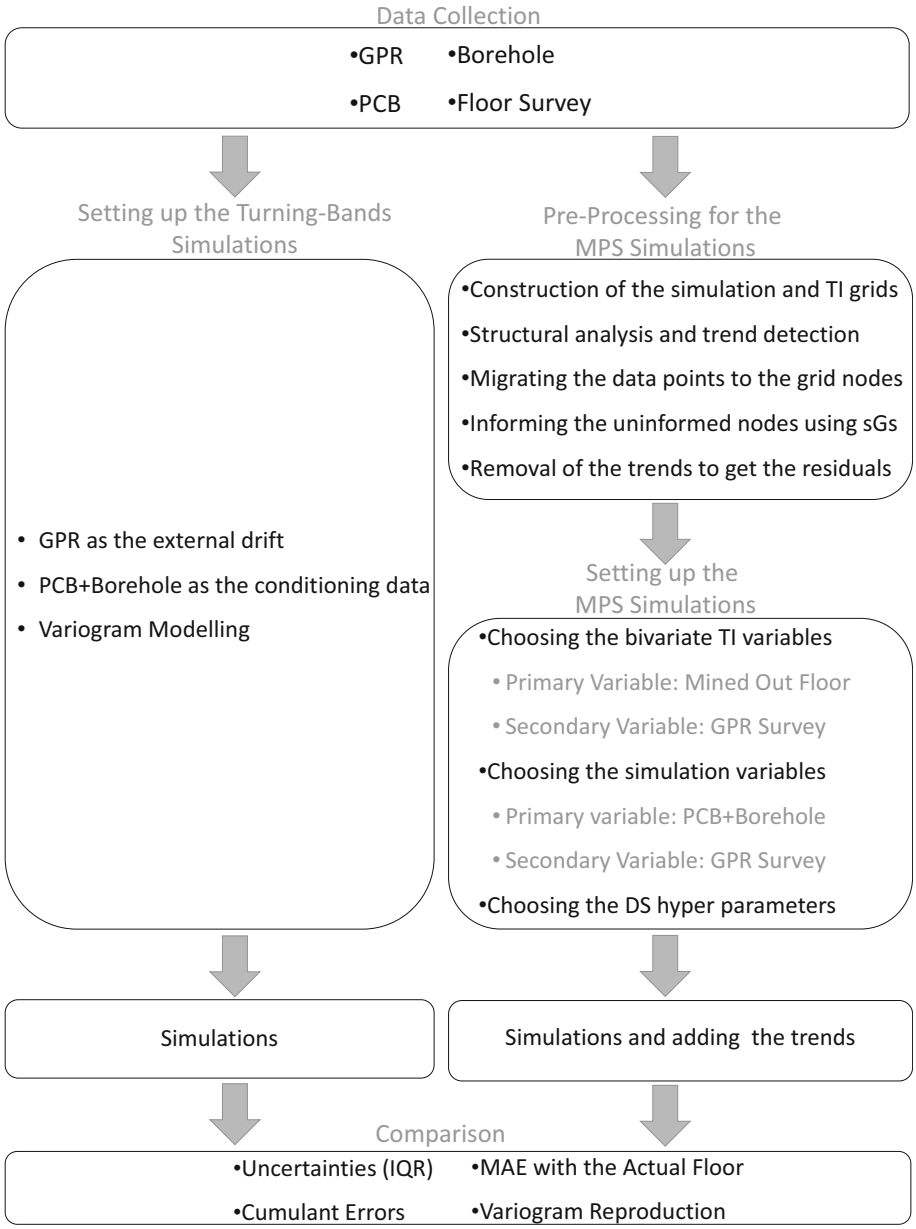

Fig. 3 Flowchart of the overall methodology

between the profiles was 15 m and the sampling density was 1 m. The collected raw GPR data has been through a processing stage which included GPR conversion, data editing, basic processing and advanced processing (i.e., zero-time correction, de-wow, gaining, filtering and time to depth conversion). The resolution of the data processed had $\pm$ 3 cm vertical resolution. After the data processing stage, the GPR readings were converted to the elevation values of the interface, as metre being the unit.

The exploration boreholes were drilled on a regular grid of 76.2 $\times$ 76.2 m in both the Oak and Kumbur mine areas. These boreholes contain a variety of information including grades and lithologies defined in three-dimensional space. An example of these units intersected by a borehole can be seen in Fig. 1. For the sake of simplicity, the lithologies are grouped into three layers based on their Al_2O_3% and SiO_2% grades (Erten 2012). These layers comprise the top-soil, bauxite and the ferricrete units.

The number of boreholes drilled for the Oak mine is 33, and it is 13 for the Kumbur mine. In addition to the exploration boreholes, 218 saturation boreholes, also called production control boreholes (PCB) data, were drilled in the Kumbur mine area. The square grid spacings between these holes were 19.05 m, and they were only analysed for the lithologies to aid delineation of the ore boundaries. Therefore, PCB data contain only the elevation values corresponding to the bauxite/ferricrete interface. Lastly, following the extraction of the bauxite ore, the resulting

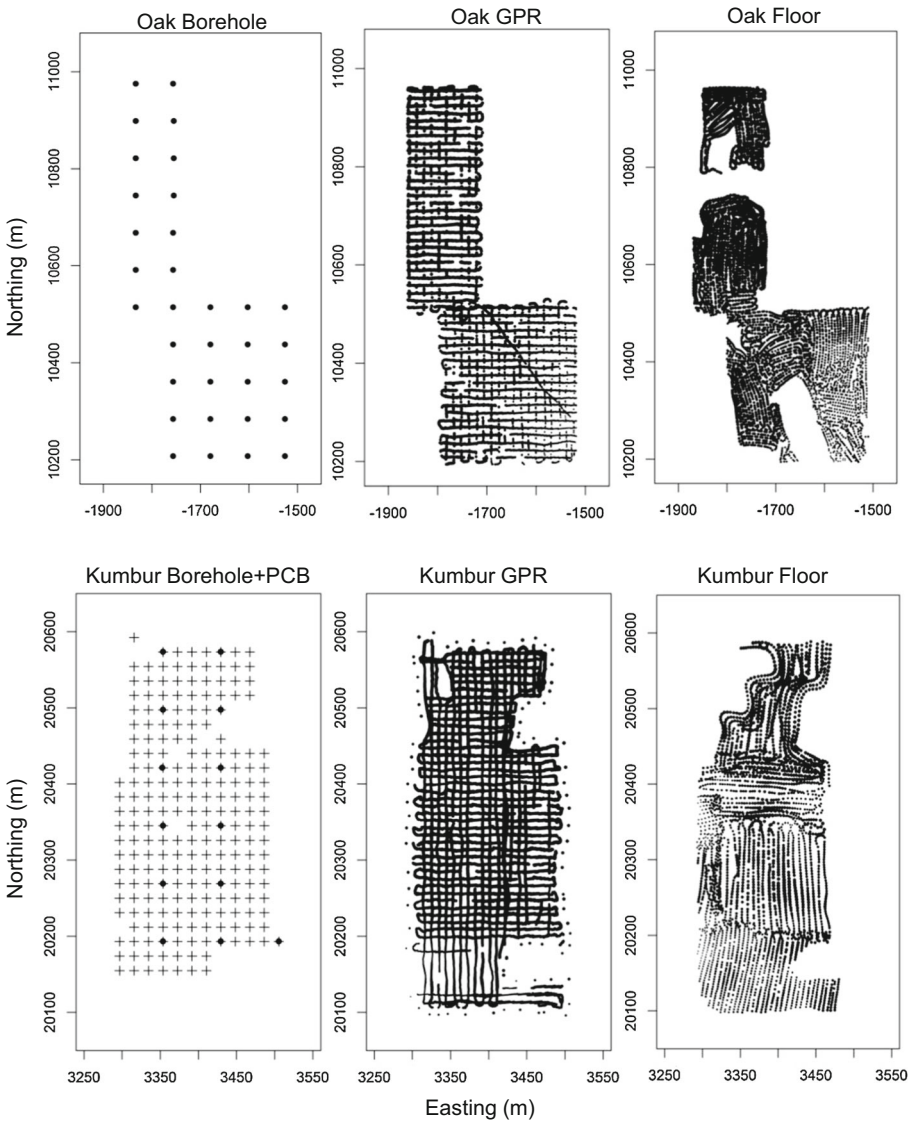

Fig. 4 Location maps of the data collected from the Oak and Kumbur mine areas. Circles in the borehole maps represent the exploration borehole locations whereas "+" signs in the Kumbur mine represent the saturation drill hole locations

mined-out surfaces were also surveyed to measure the variability in the footwall of the bauxite seam. Location maps of all the available data can be seen in Fig. 4.

3.2 Structural analysis and trend detection

In order to perform the structural analysis of the elevation variables, omnidirectional variograms were computed for both the Oak and Kumbur mine areas as shown in Fig. 5. The experimental variogram computed for the Oak mine indicates the existence of a spatial trend, as the variogram is not bounded and does not have a finite sill. Therefore, the geological interface between the bauxite/ferricrete units must be modelled by a non-stationary random function. As for the Kumbur mine, the variograms also exhibit a non-stationary behaviour. However, the non-stationarity for this mine seems to be not strong and the rise in the variogram values tends to stop and drop down after a lag distance of 450 m. Therefore, the intrinsic hypothesis can still be used in this case.

Optimal determination of the trends was performed using the non-stationary modelling tool of the ISATIS software (Bourassi et al. 2016). The three types of trends that were tested were the universality condition (no trend), the linear trend (1, x, y) and the quadratic trend (1, x, y, x^2, y^2, xy). For the Oak mine variables, the linear trend was found to be optimal whereas for Kumbur, a quadratic trend was the most appropriate. The trend coefficients, which were estimated by the method of least squares, are presented in the supplementary material. These coefficients are used to construct the trend surfaces to obtain the residuals for the MPS simulations.

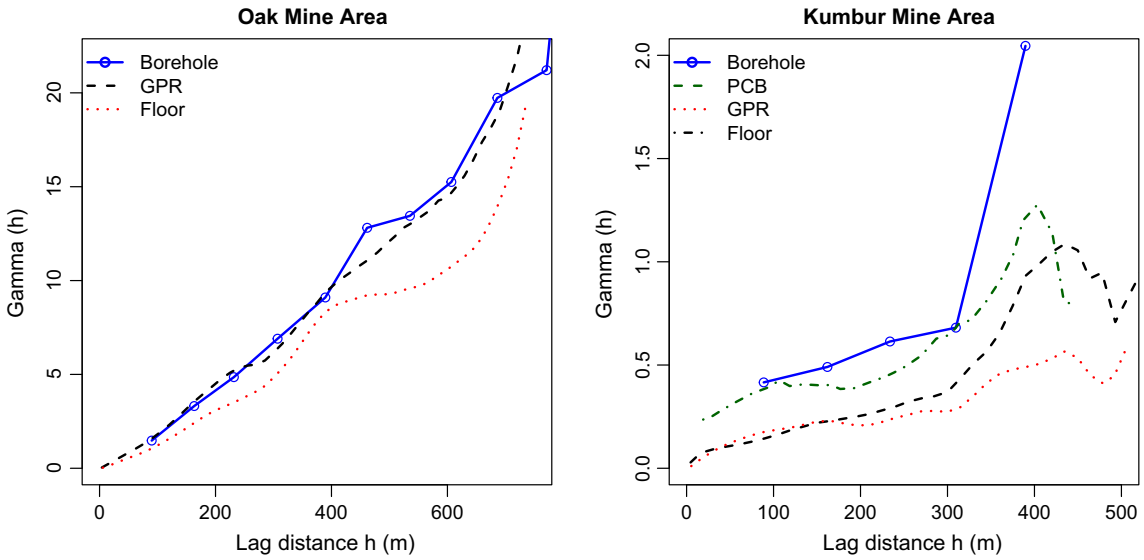

Fig. 5 Omnidirectional variograms computed for the Oak and Kumbur mine areas

3.3 Migration of the data points to the grid nodes

To be able to use the data in the MPS simulations, the secondary variable and the selected TI should be defined on predefined grid nodes. Given that the collected raw data is in the form of punctual data, they should be migrated to the nodes of a defined grid. For this purpose, two grids for both mine areas were created. The single cell size (pixel) of the created grid was chosen as 2.38×2.38 m. The size of the constructed grids were 180×400 for the Oak mine and 97×214 for the Kumbur mine.

Although the GPR pick-points and the floor survey points were densely sampled in both mine areas, they were collected at irregular finite locations. Hence, once the data points are migrated to the closest grids nodes, some of the nodes may still be uninformed. To create a complete TI out of the GPR and floor survey data, these nodes should be informed. This task can be achieved by interpolating the elevation values at the uninformed grid node locations. However, interpolation techniques such as kriging leads to a smoothing effect and the resulting statistical properties of the re-constructed images would be different to those of the raw data used. Geostatistical simulation techniques, such as the sequential Gaussian simulation (sGs), on the other hand, can successfully be used to assign the elevation values to the uninformed grid nodes. An illustration of the re-construction process can be seen in Fig. 6.

The benefit of using a geostatistical simulation technique is that the variogram and the statistical properties of the resulting realisation are preserved. A drawback could be the loss of multiple-point statistical information while simulating the values using a variogram model. However, since the original data set is rather dense, it is thought that the majority of the grid nodes are informed by the raw data points prior to the simulations. Hence, the degree of multiple-point statistical loss that can occur is considered negligible, and the created realisations are still believed to retain the inherent higher-order statistics.

A significant factor that can have an impact on the simulated values could be the trends apparent in the datasets. Nevertheless, since the GPR and floor surveys data points are dense, the raw data points used to simulate the uninformed nodes always stay within the close proximity. Therefore, the influence of trend on the assigned values is not critical. This has also been confirmed by the study in which the the elevation variable from GPR data was reproduced using both stationary and non-stationary geostatistical modelling techniques (ordinary kriging, universal kriging and IRF-k) (Dagasan et al. 2018a). The results of the study demonstrate that all the techniques yielded rather similar performances due to the abundance of data points. Hence, the variograms to perform the sGs simulations in this study were obtained by fitting a model to the experimental variograms computed along the trend-free directions.

Identification of the trend-free directions was performed by first computing the variogram maps of the raw data points. The variogram map illustrated in Fig. 7b, for instance, was computed for the GPR Kumbur variable and pointed out the trend-free direction as N130°. The experimental variogram calculated along the trend-free direction can also be seen in Fig. 7a. The model fitted to this variogram is composed of two spherical structures, the ranges of which were 19.33 m and 306.05 m, respectively. The sills of the variogram, on the other hand, were 0.065 m^2

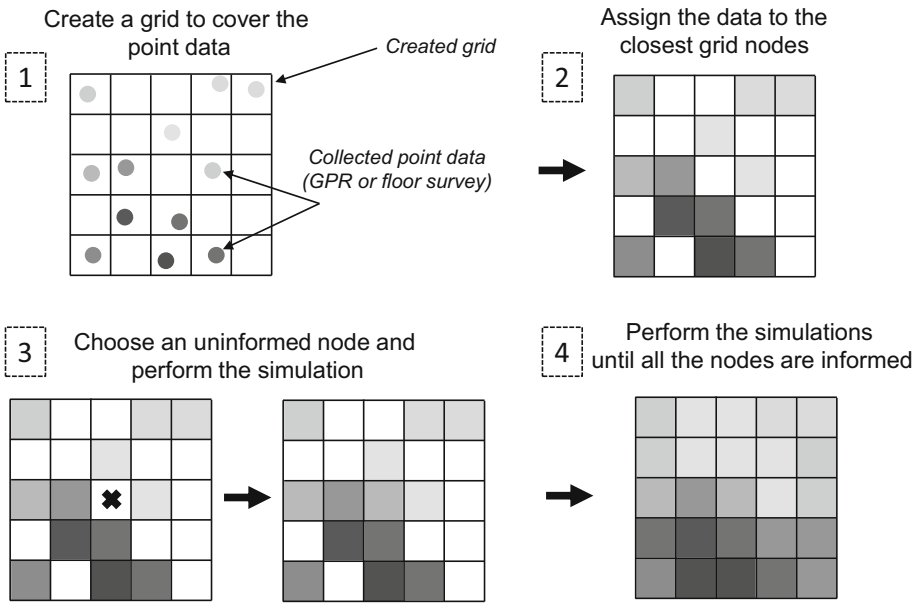

Fig. 6 Process used to both convert the point data into the gridded type and reconstruct the images

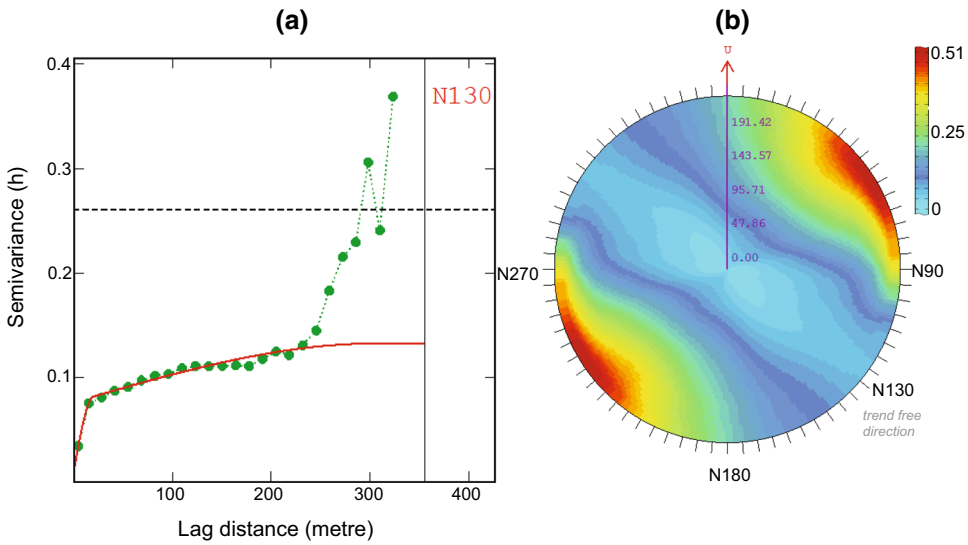

Fig. 7 **a** Experimental variogram calculated along the trend-free direction (N130°) and the variogram model fitted for the Kumbur GPR variable **b** variogram map of the Kumbur GPR variable

and 0.056 m^2, respectively. The procedure described here was utilised for the reconstruction of the Kumbur floor survey, Oak GPR and floor surveys as well, which are provided in the supplementary material.

4 Setting up the MPS simulations

MPS simulations in this study were carried out using the Direct Sampling (DS) algorithm (Mariethoz et al. 2010). The benefit of using the DS algorithm is that it does not store the patterns to retrieve the conditional probabilities as in other algorithms. It instead scans the TI until a compatible pattern is found. Therefore, the simulations are performed rather fast. Another useful feature of DS is that it allows multivariate simulations utilising the multiple-point dependence between given variables. Readers are referred to Mariethoz et al. (2010) for the details of the algorithm and Meerschman et al. (2013) for a guide on selecting the algorithm input parameters.

4.1 Choosing the simulation variables

Two types of exploration data were utilised to model the orebody boundaries. The first one of these was the PCB data collected on a regular grid. The second one was the GPR survey, which was originally collected in the form of two-way travel time (the unit is in m/ns). However, during the processing stage, the unit was converted into metres, which represents the elevation variable of the footwall

contact. The GPR data originally indicated the depth from the surface to the geological interface. Having subtracted the GPR depths from the surface elevations, the elevation variable of the geological interface was obtained.

Of the available exploration data collected from both mine areas, GPR has been used as an auxiliary variable to guide the simulations. It acts as a soft data and is considered to be useful to improve the estimations and deal with the non-stationarity (Rezaee and Marcotte 2017; Zhang et al. 2015). On the other hand, the borehole and the PCB data were used as hard data to condition the simulations. Migrating the conditioning data to the grid nodes was performed internally by the DS algorithm prior to the simulations. Since the borehole and PCB data were drilled on a regular grid (equally spaced), they are co-located with the created grid nodes. Therefore, no shift in the locations took place while migrating the points.

Simulations were planned to be of two types: (1) univariate and (2) bivariate. For the univariate case, the mined-out surveys of both mines are used as TIs. As for the bivariate simulations, bivariate TIs were constructed to utilise the multiple-point dependence between the variables. The mined-out survey data was selected for the primary variable of the TI and the GPR data was selected for the secondary component of the TI. Components that make up the bivariate simulations can be seen in Fig. 8.

4.2 Algorithmic input parameter selection

In addition to the simulation and TI variables, the DS requires the specification of some algorithm input parameters to perform the simulations. Although the latest version of the DS, which is DeeSse, is comprised of numerous features and parameters, only the parameters utilised in this research are explained here. Other parameters were, therefore, kept as their default values.

Five parameters were chosen to perform the preliminary sensitivity analysis for the bivariate simulations. These parameters were the weight factor w_{hd} attached to the conditioning data, acceptance threshold (t_{hd} and t_{GPR}), and the number of neighbours (n_{hd} and n_{GPR}) of the DS algorithm. The weighting factor w_{GPR} of the GPR data was not selected for the sensitivity analysis, as the simulation grid SG_{GPR} of the GPR data was already exhaustively informed and therefore any change in w_{GPR} would not affect the simulations. In addition, the scan fraction f, being one of the main parameters of the DS, was also not considered for the sensitivity analysis as the initial tests had shown that it has an insignificant effect on the simulation quality for this case. Therefore, f was kept equal to 0.5 throughout the simulations. The chosen value is also consistent with the suggested values presented in Meerschman et al. (2013) for continuous simulations.

Based on the sensitivity analysis performed with a set of input parameter combinations, the best simulation parameters were determined. Further automatic tuning of the

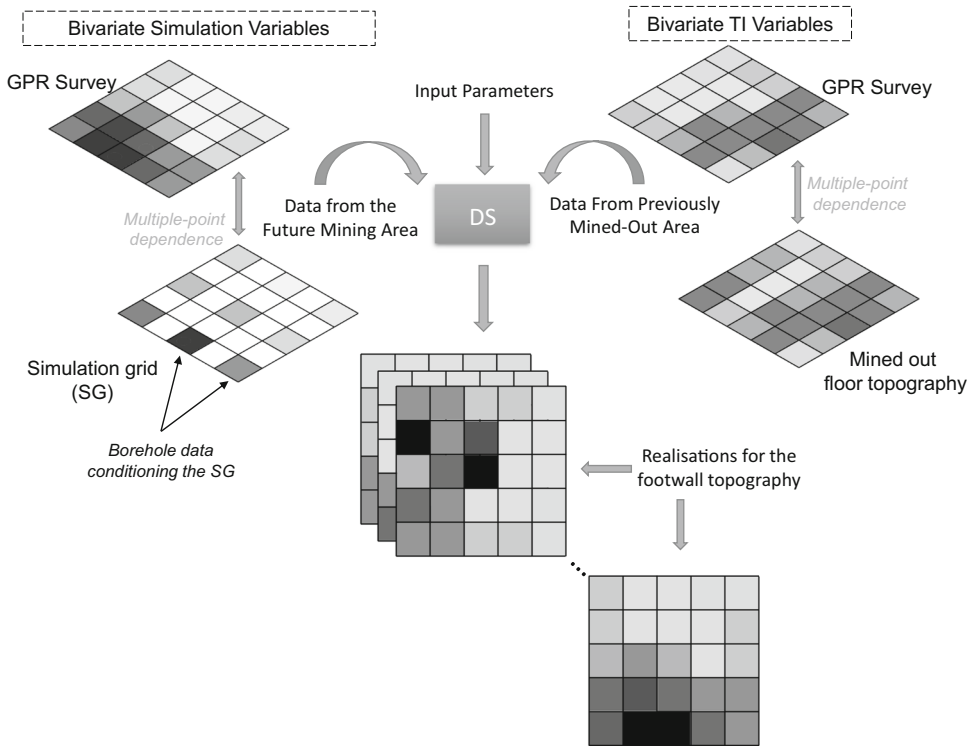

Fig. 8 Inputs and outputs of the bivariate DS simulations

parameters was performed using the approach presented in Dagasan et al. (2018b). The method first computes the multiple-point statistics of the patterns retrieved from the conditioning data and compares the statistics of the resulting realisation after each iteration of the parameter set. After several hundreds of parameter trials, the method gives the set of chosen parameter values yielding least dissimilarity value. Table 1 illustrates the tuned input parameters. Parameters that are used to perform the univariate and bivariate simulations for both mine areas can be seen in Table 2.

5 Results and discussion

5.1 Results

Results of the MPS simulations were analysed using 40 univariate and bivariate realisations generated for each mining area. In addition, produced MPS simulations were also compared with the classical geostatistical simulations performed using the Turning Bands method (TB) (Matheron 1973). Due to space limitations, only the bivariate simulation results for the Kumbur mine were presented in the paper. The remaining analyses can be found in the supplementary material attached to the online version of this document.

The MPS simulations were performed using the residuals of the simulation and TI variables. First, each of the trend surfaces was subtracted from the original dataset. These residuals were then used as the simulation and TI variables to perform the MPS simulations. The TI and the simulation variables used can be seen in Fig. 9. Following the generation of 40 realisations, the trend surface of the PCB data was added back to each of the realisations.

Geostatistical simulations, on the other hand, were performed using TB with the external drift kriging method in the RGeostats package (Renard et al. 2017). Having defined the GPR variable as an external drift, the residuals of the PCB data were obtained to fit a variogram model. The experimental variogram computed along different directions revealed the existence of a geometric anisotropy. The main anisotropy directions were identified as N0° and N90°. The fitted models comprised of two nested exponential and spherical structures, as can be seen in Fig. 10. The spherical component has a sill value of 0.137 m^2 and has a range of 112 m in the N0° direction and 237 m in the N90° direction. The sill value of the exponential component, on the other hand, is 0.2 m^2 and the ranges are 38 and 35 m in N0° and *N*90° directions, respectively. For the simulations, the number of turning bands used was 400. 40 TB realisations were generated using this set-up. The first three realisations of the DS and TB simulations can be seen in Fig. 11. The average of 40 realisations along with their variograms are given in Fig. 12.

Table 2 DS parameters for the Oak and Kumbur mine areas

Parameters	w_{hd}	n_{hd}	n_{GPR}	t_{hd}	t_{GPR}
Kumbur bivariate	13.08	14	45	0.009	0.305
Kumbur univariate	13.08	14	–	0.009	–
Bivariate Oak	10.00	20	21	0.001	0.01
Univariate Oak	10.00	6	–	0.001	–

Assessment and performance comparison of the two methods have been carried out using several statistical indicators. The first and perhaps the most interesting one is the reproduction of two-point statistics of the conditioning data used. Omnidirectional variograms presented earlier in Fig. 9 show that the variograms of the residual TI and the simulation variables are noticeably different. Therefore, it would be fair to expect that the TI and the simulation variables were not very compatible. However, despite such a difference observed in Fig. 9, variograms of the realisations shown in Fig. 12 reveal that the DS was able to reproduce the two-point statistics of the PCB data with success.

In order to visually observe the differences between the simulations, the average of the simulations and the fluctuation of the simulated values around the mean value at each grid node were analysed. Given all the created L realisations, the E-type maps were calculated by averaging all the simulated values at each x grid node location, as in the following:

$$z_E^*(x) = \frac{1}{L}\sum_{l=1}^{L} z^l(x) \tag{1}$$

where $z_E^*(x)$ represents the expected elevation values at x locations and $z^l(x)$ represents those for the lth realisation. As far as these maps for the DS and TB simulations are concerned, there exists a slight difference between them.

Table 1 Optimised DS parameters used for the Kumbur simulations (Dagasan et al. 2018b)

Parameters	w_{hd}	n_{hd}	n_{GPR}	t_{hd}	t_{GPR}
Tuned Kumbur bivariate simulations	13.08	14	45	0.009	0.305

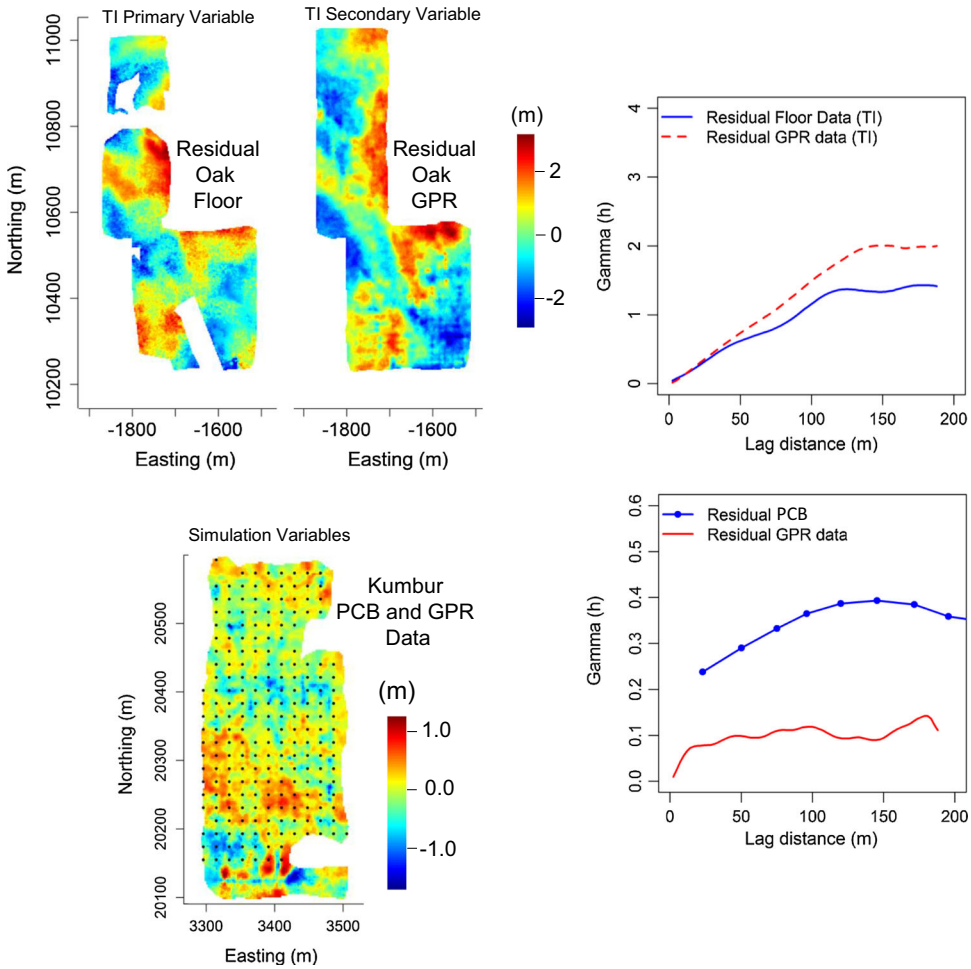

Fig. 9 Bivariate training image, simulation variables and their omni-directional variograms for the bivariate Kumbur mine area simulations. Black points overlain the GPR residual map indicates the conditioning data point locations

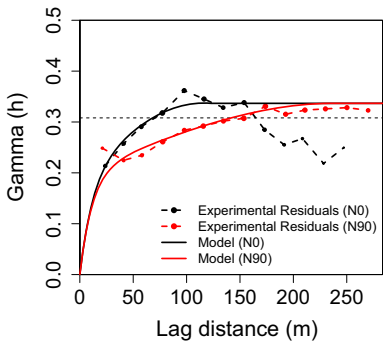

Fig. 10 Experimental variogram of the PCB residuals along with the fitted model

Therefore, it can be concluded that the average of the simulations are rather similar.

The fluctuations around the mean were used to assess the resulting model of uncertainty. To quantify this, the interquartile-range (IQR) of the simulated values at each grid node was calculated. This was simply performed by taking the difference between the upper and lower quartiles of the simulated values as in the following:

$$q_R(x) = q_{0.75}(x) - q_{0.25}(x) \quad (2)$$

Unlike the E-type maps, the difference in the IQR maps is rather obvious, as can be seen in Fig. 12. These maps and the distribution of the IQR values at each grid node show that the DS produces less uncertainty. The averages of the IQR values are 0.426 for the DS and 0.501 for the TB simulations.

Another comparison has been made using the reproduction of the higher-order statistics through spatial cumulants. In order to perform this comparison, the experimental higher-order statistics were computed using the *hosc* software (Dimitrakopoulos et al. 2010). An L-shaped template was constructed along the N0° and N90° directions to calculate the third-order cumulants. The lag separations in each direction were chosen as 2.38 and the cumulants were calculated for 50 lag distances in each direction. The cumulant maps constructed for both the simulations and the reference mined-out surface of the Kumbur mine can be seen in Fig. 13.

Computed cumulant maps appear to be different and do not seem to provide an insight into the similarity between

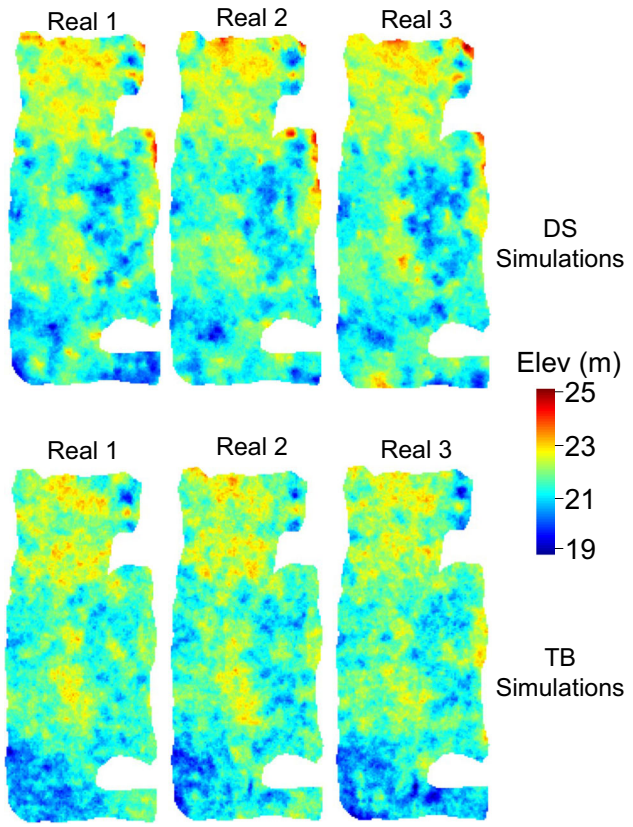

Fig. 11 First three realisations of the DS and TB simulations

the reference image and the generated realisations. Therefore, a measure is needed to be used to quantify the similarities between the images. Calculation of such a similarity was performed by pixel-by-pixel subtraction of the cumulant map of the mined-out surface from those of 40 realisations as in the following equation:

$$error_C^l = \frac{1}{N}\sum_{j=1}^{N}\left|c^l(j) - c^{(ref)}(j)\right| \tag{3}$$

where $c^l(j)$ and $c^{(ref)}(j)$ represent cumulant values at the jth pixel of the cumulant maps and N represents the total number of pixels in the cumulant maps.

The means of the calculated cumulant errors of 40 realisations are both 5×10^{-7}, hence the same. Therefore, simulations produced by both methods yield rather similar multiple-point statistics of the mined-out area. A more direct similarity between the realisations and the reference mined-out surface was calculated by subtracting the realisations from the reference image pixel-by-pixel for K number of grids and averaging the differences:

$$error_{Ref} = \frac{1}{LK}\sum_{l=1}^{L}\sum_{i=1}^{K}\left|Z^l(i) - Z^{(ref)}(i)\right| \tag{4}$$

$Z^l(i)$ and $Z^{(ref)}(i)$ represent the elevation variable of the lth realisation and the reference mined-out surface. The mean absolute error found in such a calculation is 0.534 for the TB and 0.528 for the DS simulations. This measure also shows that there is not a significant difference between the DS and the TB simulations for this specific case.

Analyses presented above have also been performed for univariate Kumbur, Bivariate Oak and Univariate Oak simulations. Although the detailed result can be found in the supplementary material, a summary of the important points are given in Table 3. The results show that the DS tends to yield less uncertainty. For the cumulant errors, the DS gives smaller cumulant errors in three out of four comparisons. This is an expected outcome as the DS reproduces multiple-point statistical information. Concerning the direct comparison made with the reference mined topography, the DS gives two better results and one similar result with the TB method.

5.2 Discussion

Considering the mining method of such deposits, a new mined-out floor is always exposed following the extraction of a bauxite unit at a certain location of the mine site. Thus, one can generate a catalogue of training images from all the formerly mined-out areas to simulate the future mining locations. Having formed such a database, the geologists can have a variety of training images to choose from. This would allow them to readily find a compatible TI that matches the expected spatial variability of the orebody boundaries in a future mining area. Another benefit of the use of MPS would be the use of a non-parametric approach for the spatial continuity. The use of TI makes it easier for the non-expert users as the structural information is not expressed in a mathematical definition.

Equipment selectivity can also have an effect on the quality of the TIs generated. A front-end loader type of mining equipment is used to extract the deposit, and the selectivity of the equipment hinders accurately following the fluctuations of the interface (Dagasan et al. 2018c). Therefore, the created TIs might also include subjectivity such as operator error and limited equipment selectivity. To alleviate this problem, a pilot area near a future mining location can be excavated with more selective mining equipment to expose the geological variations for better quality TIs. In other words, mining machinery with a smaller bucket would allow better exposure of the true geological variations. A TI produced following such detailed excavation is believed to improve the quality of the MPS simulations.

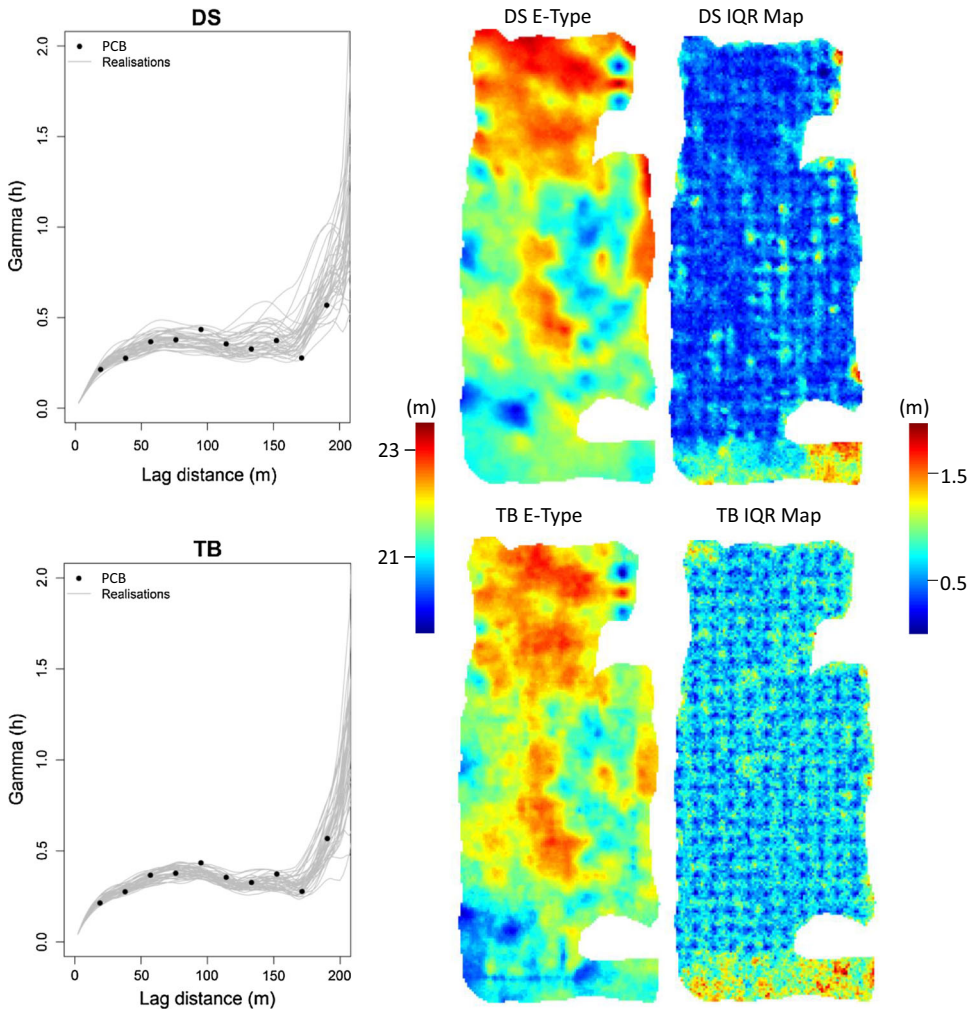

Fig. 12 Average of the TB and DS realisations together with the IQR maps and the variograms of the realisations

6 Summary and conclusions

This paper investigated the application of MPS in modelling the geological contact topography within a lateritic bauxite mine. The step-by-step methodology to perform univariate and bivariate simulations was proposed using the Direct Sampling (DS) multiple-point statistics algorithm; which involved borrowing bivariate training images (TI) from an analogue site where the mined-out floor surfaces as well as the GPR survey were available.

The resulting DS simulations were compared with classical geostatistical simulations obtained with the Turning Bands (TB) method. The comparison has been made using several statistical indicators. In terms of the performance measures, the observed differences between the TB and the DS simulations were fairly small; the results of both simulation techniques were quite similar.

The approaches were, however, rather different. On the one hand, the TB method assumes multi-Gaussianity of the random field and infers the parameters of the model from the data. This has the advantage to be straightforward and is based on a well established theory. It requires, however, some careful analysis of the data to identify properly the covariance or variogram model. On the other hand, the DS method borrows the spatial patterns from the training image which was taken from an analogue site. This allows to avoid the multi-Gaussian assumption but relies on assuming that the TI represents properly the expected spatial variability. It is important to note that the two-point statistics of the TIs were different from those of the conditioning data of the simulation area. This is usually an unwanted situation and the TI would normally be evaluated as non-compatible. Nevertheless, by adapting the parameters of the DS method, it was possible to successfully perform the simulations and reproduce the two-point statistics of the conditioning data very well. This fact shows that even if the TI is not perfectly compatible with the simulated area, the DS method is rather robust. The relation between the GPR data and the geological contact was also directly accounted for in a multivariate manner using the DS, without having to provide an explicit correlation model.

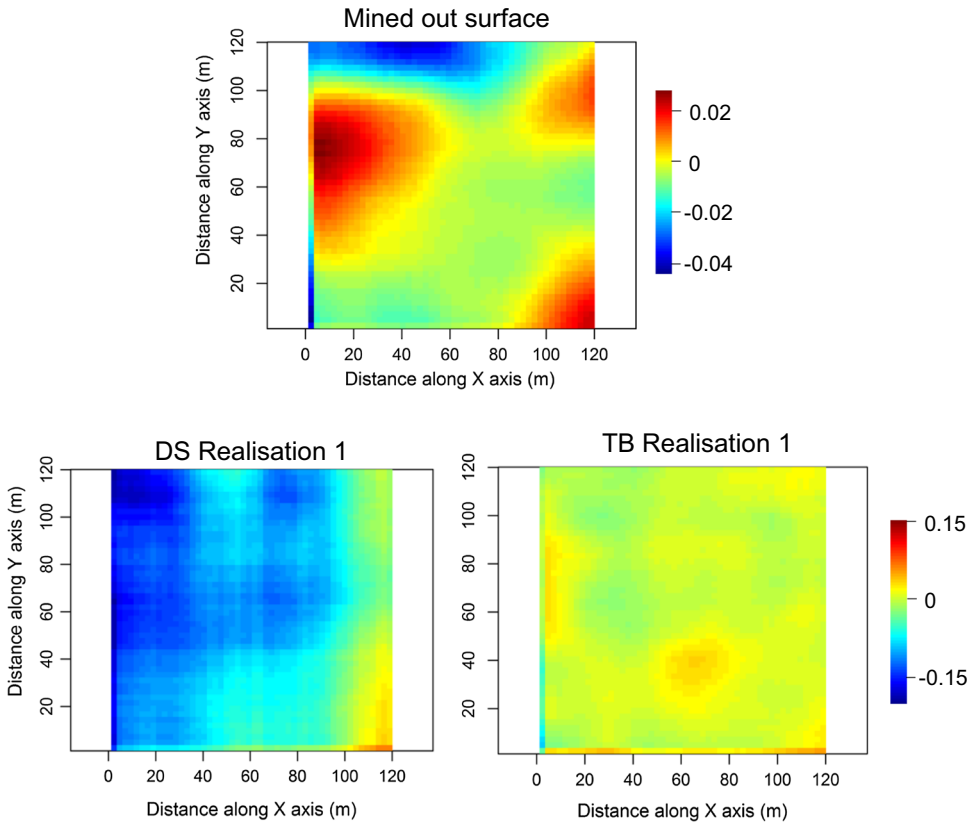

Fig. 13 Cumulant maps of the Kumbur mined-out floor and the first realisations of the DS and TB Kumbur simulations

Table 3 Summary of the simulation results

Simulation type	Mine area	Method	Uncertainty (IQR)	Cumulant error	MAE
Univariate	Oak	DS	0.69	0.0013	0.92
		TB	0.99	0.0028	0.94
	Kumbur	DS	0.48	1.5e−6	0.54
		TB	0.52	3.0e−7	0.53
Bivariate	Oak	DS	0.80	0.0011	0.87
		TB	0.96	0.0122	0.94
	Kumbur	DS	0.43	5e−7	0.53
		TB	0.50	5e−7	0.53

In conclusion, utilising Direct Sampling to model the geological interface in lateritic mines seems to be a promising approach that can be incorporated in resource estimations. It provides a framework in which one can relax the multi-Gaussianity assumption. It allows integrating the data from an analogue site in a straightforward manner, even if the training data is not perfectly in agreement with the conditioning data set.

Acknowledgements The authors would like to thank Ilnur Minniakhmetov and Ryan Goodfellow from the Department of Mining and Materials Engineering of McGill University for providing the *hosc* software and their kind help.

References

Abzalov MZ, Bower J (2014) Geology of bauxite deposits and their resource estimation practices. Appl Earth Sci 123(2):118–134

Arpat GB, Caers J (2007) Conditional simulation with patterns. Math Geol 39(2):177–203

Bardossy G, Szabo IR, Varga G (2003) A new method of resource estimation for bauxite and other solid mineral deposits. Berg Und Huttenmannische Monatshefte 148(2):57–64

Bastante FG, Taboada J, Alejano L, Alonso E (2008) Optimization tools and simulation methods for designing and evaluating a mining operation. Stoch Environ Res Risk Assess 22(6):727–735

Bourassi A, Foucher B, Geffroy F, Marin JY, Martin B, Meric YM, Perseval S, Renard D, Robinot L, Touffait Y, Wagner L (2016) Isatis software user's guide. Geovariances, Ecole des Mines de Paris, Paris

Dagasan Y (2018) Development of a grade control technique optimizing dilution and ore loss trade-off in lateritic bauxite deposits. PhD Thesis, Curtin University, Curtin

Dagasan Y, Erten O, Topal E (2018a) Accounting for a spatial trend in fine-scale ground-penetrating radar data: a comparative case study. J South Afr Inst Min Metall 118(2):173–184

Dagasan Y, Renard P, Straubhaar J, Erten O, Topal E (2018b) Automatic parameter tuning of multiple-point statistical simulations for lateritic bauxite deposits. Minerals 8:220

Dagasan Y, Renard P, Straubhaar J, Erten O, Topal E (2018c) Pilot point optimization of mining boundaries for lateritic metal deposits: Finding the trade-off between dilution and ore loss. Nat Resour Res 28:153–171

Davis JL, Annan AP (1989) Ground-penetrating radar for high-resolution mapping of soil and rock stratigraphy 1. Geophys Prospect 37(5):531–551

de Freitas Silva M, Dimitrakopoulos R (2016) Simulation of weathered profiles coupled with multivariate block-support simulation of the puma nickel laterite deposit, brazil. Eng Geol 215:108–121

De Iaco S, Maggio S (2011) Validation techniques for geological patterns simulations based on variogram and multiple-point statistics. Math Geosci 43(4):483–500

Dimitrakopoulos R (1998) Conditional simulation algorithms for modelling orebody uncertainty in open pit optimisation. Int J Surf Min Reclam Environ 12(4):173–179

Dimitrakopoulos R, Mustapha H, Gloaguen E (2010) High-order statistics of spatial random fields: exploring spatial cumulants for modeling complex non-gaussian and non-linear phenomena. Math Geosci 42(1):65–99

Erten O (2012) Profiling and mining control to mitigate dilution effect from SiO_2 at the base of a bauxite deposit. PhD Thesis, School of Mechanical and Mining Engineering, The University of Queensland

Erten O, Kizil MS, Topal E, McAndrew L (2013) Spatial prediction of lateral variability of a laterite-type bauxite horizon using ancillary ground-penetrating radar data. Nat Resour Res 22(3):207–227

Erten O, McAndrew L, Kizil MS, Topal E (2015) Incorporating fine-scale ground-penetrating radar data into the mapping of lateral variability of a laterite-type bauxite horizon. Min Technol 124(1):1–15

Gloaguen E, Dimitrakopoulos R (2009) Two-dimensional conditional simulations based on the wavelet decomposition of training images. Math Geosci 41(6):679–701

Goodfellow R, Consuegra FA, Dimitrakopoulos R, Lloyd T (2012) Quantifying multi-element and volumetric uncertainty, coleman mccreedy deposit, ontario, canada. Comput Geosci 42:71–78

Guardiano FB, Srivastava RM (1992) Borrowing complex geometries from training images: the extended normal equations algorithm. Stanford Center for Reservoir Forecasting Report, Stanford University, Stanford

Hartman HL, Mutmansky JM (2002) Introductory mining engineering. Wiley, Hoboken

Honarkhah M, Caers J (2010) Stochastic simulation of patterns using distance-based pattern modeling. Math Geosci 42(5):487–517

Jones P, Douglas I, Jewbali A (2013) Modeling combined geological and grade uncertainty: application of multiple-point simulation at the apensu gold deposit, ghana. Math Geosci 45(8):949–965

Journel AG (2005) Beyond covariance: the advent of multiple-point geostatistics. Geostat Banff 2004:225–233

Mariethoz G, Caers J (2014) Multiple-point geostatistics: stochastic modeling with training images. Wiley, Hoboken

Mariethoz G, Renard P, Straubhaar J (2010) The direct sampling method to perform multiple-point geostatistical simulations. Water Resour Res 46(11):1–14

Matheron G (1973) The intrinsic random functions and their applications. Adv Appl Probab 5(3):439–468

Meerschman E, Pirot G, Mariethoz G, Straubhaar J, Van Meirvenne M, Renard P (2013) A practical guide to performing multiple-point statistical simulations with the direct sampling algorithm. Comput Geosci 52:307–324

Mery N, Emery X, Cáceres A, Ribeiro D, Cunha E (2017) Geostatistical modeling of the geological uncertainty in an iron ore deposit. Ore Geol Rev 88:336–351

Osterholt V, Dimitrakopoulos R (2018) Simulation of orebody geology with multiple-point geostatistics—application at yandi channel iron ore deposit, WA, and implications for resource uncertainty. In: Advances in applied strategic mine planning, Springer, New York, pp 335–352

Pasti HA, Costa JFCL, Boucher A (2012) Multiple-point geostatistics for modeling lithological domains at a Brazilian iron ore deposit using the single normal equations simulation algorithm. In: Geostatistics Oslo, Springer, New York, pp 397–407

Pérez C, Mariethoz G, Ortiz JM (2014) Verifying the high-order consistency of training images with data for multiple-point geostatistics. Comput Geosci 70:190–205

Renard D, Bez N, Desassis N, Beucher H, Ors F, Freulon X (2017) RGeostats: geostatistical package. http://cg.ensmp.fr/rgeostats. R package version 11.0.6. Accessed 3 Aug 2017

Rezaee H, Marcotte D (2017) Integration of multiple soft data sets in mps thru multinomial logistic regression: a case study of gas hydrates. Stoch Environ Res Risk Assess 31(7):1727–1745

Rezaee H, Mariethoz G, Koneshloo M, Asghari O (2013) Multiple-point geostatistical simulation using the bunch-pasting direct sampling method. Comput Geosci 54:293–308

Rezaee H, Marcotte D, Tahmasebi P, Saucier A (2015) Multiple-point geostatistical simulation using enriched pattern databases. Stoch Environ Res Risk Assess 29(3):893–913

Robles-Stefoni L, Dimitrakopoulos R (2016) Stochastic simulation of the fox kimberlitic diamond pipe, ekati mine, northwest territories, Canada. J South Afr Inst Min Metall 116(2):189–200

Rossi ME, Deutsch CV (2013) Mineral resource estimation. Springer, New York

Straubhaar J, Renard P, Mariethoz G, Froidevaux R, Besson O (2011) An improved parallel multiple-point algorithm using a list approach. Math Geosci 43(3):305–328

Strebelle S (2002) Conditional simulation of complex geological structures using multiple-point statistics. Math Geol 34(1):1–21

Tahmasebi P, Hezarkhani A, Sahimi M (2012) Multiple-point geostatistical modeling based on the cross-correlation functions. Comput Geosci 16(3):779–797

van der Grijp Y, Minnitt RCA (2015) Application of direct sampling multi-point statistic and sequential gaussian simulation algorithms for modelling uncertainty in gold deposits. J South Afr Inst Min Metall 115(1):73–85

Zhang T, Yi D, Huang T, Li X (2015) Reconstruction of porous media using multiple-point statistics with data conditioning. Stoch Environ Res Risk Assess 29(3):727–738

Zhang T, Switzer P, Journel A (2006) Filter-based classification of training image patterns for spatial simulation. Math Geol 38(1):63–80